Transverse Phase Space Studies in TTF Photoinjector during Run 00-01: A Comparison between Simulation and Experiment

Ph. Piot, K. Floettmann, S. Schreiber, D. Sertore,
Deutsches Elektronen-Synchrotron DESY, Hamburg, GERMANY
A. Cianchi,
INFN, Laboratori Nazionali di Frascati, ITALY
and L. Catani,
INFN, Sezione di Roma II, ITALY

August 29, 2000

- TESLA-FEL 2000-04 -

Abstract

Experimental data on transverse emittance and beam density measurements for a variety of injector settings (photocathode drive-laser phase w.r.t. to peak electric field in the RF-gun cavity, magnetic fields settings of solenoids) are compared along with numerical simulations performed using the particle tracking code ASTRA [1].

1 Introduction

1.1 General Considerations

Two series of emittance measurements were performed at different times with different methods at the TTF photoinjector. The injector beamline (see Fig. 1), up to the location where the emittance measurements were performed, consists of an rf-gun with a splitted "emittance compensation" solenoid [2] followed by a superconducting 9-cell TESLA-type accelerating cavity (referred as "booster" cavity hereafter) and a set of focusing elements (quadrupoles doublets and triplets). The emittance measurements were performed behind the booster cavity at an energy of 16 MeV approximately.

The first series, was acquired on Dec 15 and Dec 17th, 1999. At that time, the transverse emittance was measured for different photocathode drive-laser phase and for different settings of the two gun-solenoids. The emittance measurements were performed with a so-called pepperpot, a multislit mask which samples the incoming space-charge-dominated beam into emittance-dominated beamlets whose divergences are analyzed downstream,

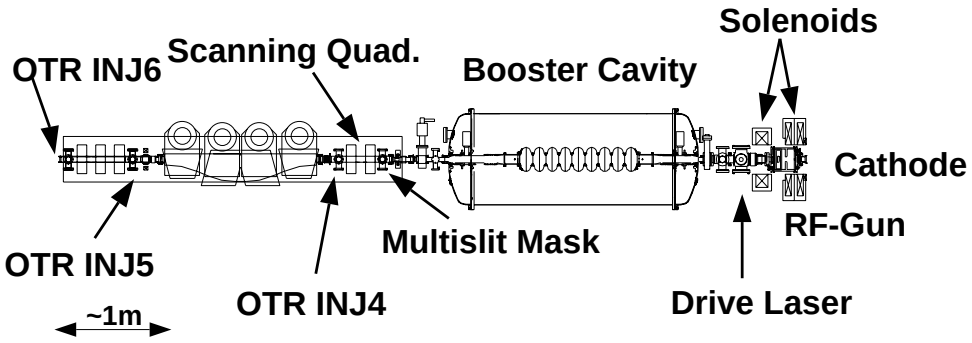

Figure 1: *Overview of the TTF-photoinjector.*

after a drift of proper length to allow the transverse momentum of the beamlets to impart a significant contribution to the transverse beamlet size.
The error bars reported for these measurements have been estimated using a simple model: we computed the resolution in the image (OTR) plan to be approximately $\Delta\sigma_y$ =60 μm; this results in an angular resolution of $\Delta\sigma'_y$ =160 μrd. The systematic error on the (unnormalized) emittance is therefore estimated as the quantity: $\Delta\tilde{\varepsilon}_y = \sigma_y\Delta\sigma'_y + \sigma'_y\Delta\sigma_y$. A much thorough analysis should be done in the analysis program by computing the errors using error propagations. Statistical errors have been estimated, for each measurement, by performing at least three measurements and were generally found to be small compared to systematics.

The second series of measurements (Jan 6-7th, 2000) utilizes the "quadrupole scan" technique, an envelope fitting method, that consists in measuring the beam rms width downstream a quadrupole whose strength is varied. This method is valid provided the transverse dynamics is emittance-dominated (i.e. single-particle dynamics is valid), an assumption that needs further elaboration since in the TTF-injector space-charge contribution to the beam envelope can be significant. Typically the coupled rms envelope evolution is described by coupled ordinary differential equations of the form [3]:

$$\begin{aligned}\sigma''_x + \kappa_x^2\sigma_x &= \frac{I}{\gamma^3 I_0(\sigma_x+\sigma_y)} + \frac{\tilde{\varepsilon}_{x,n}^2}{\sigma_x^3\gamma^2}\\ \sigma''_y + \kappa_y^2\sigma_y &= \frac{I}{\gamma^3 I_0(\sigma_x+\sigma_y)} + \frac{\tilde{\varepsilon}_{y,n}^2}{\sigma_y^3\gamma^2}\end{aligned} \qquad (1)$$

where $\sigma_{x,y}$ are the transverse rms beam size, I and I_0 are the peak and the Alfèn current respectively, $\kappa_{x,y}$ accounts for the transverse external focusing. γ is the reduced energy. The right hand side of Eqn.(1) describes the space-charge defocusing effect (first term) and "emittance pressure" (second term). In order to assess whether the space-charge term significantly contributes to the beam envelope evolution, we shall calculate the space-charge-over-emittance ratio defined as (e.g. for x-plane): $R_x = I/[I_0(\sigma_x+\sigma_y)\gamma]\times(\sigma_x^3/\tilde{\varepsilon}_{x,n}^2)$. This ratio, for a longitudinally gaussian charge density, takes the form:

$$R_x = \frac{Q}{I_0(\sigma_x+\sigma_y)\gamma}\times\frac{c}{\sqrt{2\pi}\sigma_z}\times\frac{\sigma_x^3}{\tilde{\varepsilon}_{n,x}^2} \qquad (2)$$

where we have introduced the bunch length σ_z and the bunch charge Q; the same type of relation yields for the y-plane by interchanging the subscript $_x$ and $_y$. From Eqn.(2)

we can derive a relation between σ_x, and σ_y for the beam to be dominated by emittance pressure ($R_x \ll 1$), we must have:

$$\frac{\sigma_x^3}{\sigma_x + \sigma_y} \ll \frac{\sqrt{2\pi}\sigma_z}{c} \frac{\gamma I_0 \tilde{\varepsilon}_{x,n}^2}{Q} \tag{3}$$

In the post-booster cavity region, emittance and space charge term contribution in the envelope equation can be of the same order (typically $R_x \simeq 1$) and therefore, under axi-symmetric assumption ($\sigma_x = \sigma_y$), the beam spot size should have a typical transverse beam size of $\sigma_x < 1\,\mathrm{mm}$ (this number is estimated assuming a longitudinal bunch length of σ_z =2 mm, $\tilde{\varepsilon}_x$ =8 mm-mr, Q =1 nC, $\gamma = 34$) [1]. It is interesting to numerically simulate a quadrupole scan, using the particle tracking code ASTRA, and quantify the validity of the method as the beam is not yet fully thermalized. For such a purpose we scan the quadrupole strength (as done experimentally on Jan-2-00) of quadrupole Q1.INJ1 (located at z =2.81 m), with all the quadrupoles between Q1.INJ1 and the observation point unexcited, and record the transverse beam sizes at the location of the OTR monitor INJ5 (located at z =5.38 m from the photocathode). The results of the numerically-performed quadrupole scan along with the fit of this scan are presented in figure 2; it is noticed that

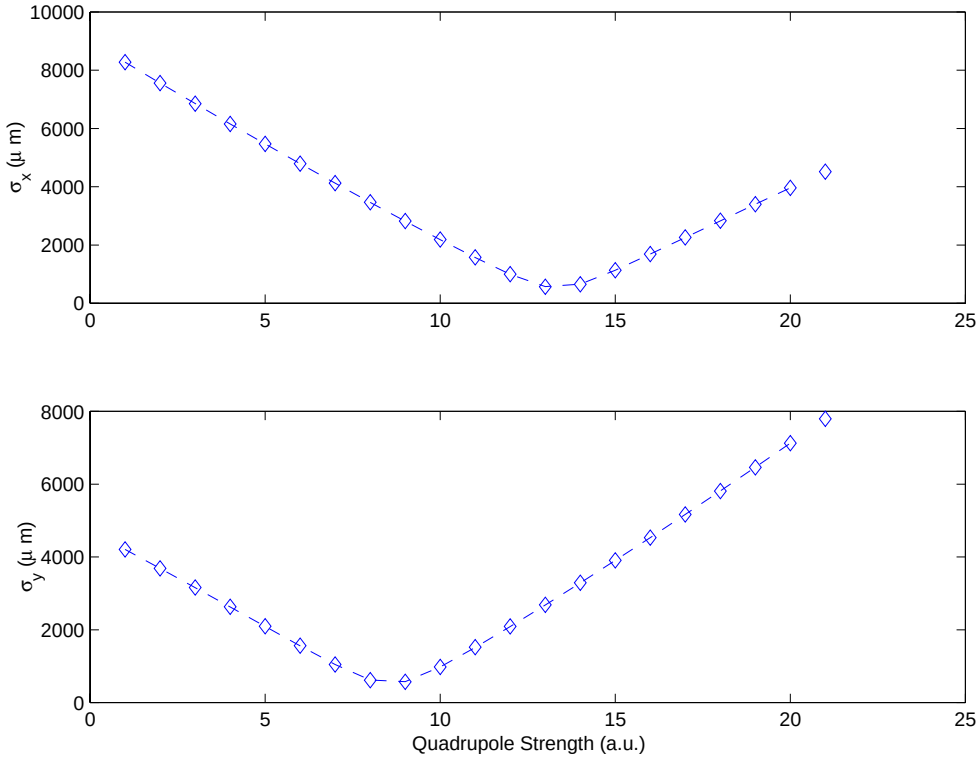

Figure 2: *Horizontal (top) and vertical (bottom) rms beam size variation versus excitation of quadrupole Q1.INJ1. The diamonds represent simulated measurement points and the dashed line is the fit from which the beam parameters are computed (see Table 1).*

the recovered emittance values from the fit are within ≃12% in agreement with the initial

[1] In the simulation presented in this section, the beam spot size variation during the quadrupole scan took values as large as 6 mm, and the emittance measurement was not significantly affected; probably because the criterion Eqn.(3) is quite conservative.

emittance, further comparison between the Twiss parameters are gathered in Table 1, again, good agreement is observed. Such agreement validates the use of the quadrupole scan method in the injector as long as the transverse rms beam size is kept below approximately 1 mm.

This latter point needs further elaboration. If we compare the simulation of the

Parameter	ASTRA	SIMULATED MEASUREMENT	units
$\beta\gamma\tilde{\varepsilon}_x$	6.02	6.30±1.56	mm-mr
α_x	-1.21	-1.25±0.34	–
β_x	3.30	3.03±0.62	m
$\beta\gamma\tilde{\varepsilon}_y$	5.63	5.80±1.43	mm-mr
α_y	-1.25	-1.25±0.33	–
β_y	2.85	2.91±0.53	m

Table 1: *Comparison between emittance from* ASTRA *input and recovered emittance after simulating a quadrupole scan-based emittance measurement in the injector.*

quadrupole scan method with and without the contribution of space charge[2], see Figure 3, we notice that even when the space charge routine is turned off, there is still substantial emittance variation during the quadrupole scan measurement, while the beam spot size variation is identical. This observed emittance variation is indeed attributed to chromatic effects as it can be seen in Fig.4, where we present the emittance and beam envelope evolution versus the gradient of the scanned quadrupole Q1.INJ1 for various incoming beam rms energy spread. The estimated energy spread, at the time of our experimental measurement, is estimated to approximately 150 keV since the booster cavity was operated for providing maximum energy gain (and not for minimum energy spread). Chromatic effects, in the present case, are caused by the quadrupole whose strength is inversely proportional to the beam longitudinal momentum, so that, to first order, the focusing strength for a given electron with a relative momentum offset δ w.r.t. the reference trajectory writes: $k = k(1 - \delta + \mathcal{O}(\delta^2))$. In order to explain our numerical observation by means of chromatic effects, we first approximate the quadrupole as a thin lens, so that the first order transfer matrix from the quadrupole entrance plane up to the observation point (i.e. OTR INJ.5) writes:

$$R = \begin{pmatrix} 1 + klL(1-\delta) & L \\ k(1-\delta) & 1 \end{pmatrix} \tag{4}$$

where k is the quadrupole strength (in m^{-2}), l its magnetic length, and L the drift length from the quadrupole exit plane up to the OTR screen.
The propagation of second order moments in the (x, x') phase space, taking into account the rms relative energy spread $\langle\delta^2\rangle^{1/2}$, yields at the observation point:

$$\begin{aligned} \langle x^2\rangle &\overset{\text{def}}{=} \langle x^2\rangle_{\delta\neq 0} = \langle x^2\rangle_{\delta=0} + (klL)^2\langle\delta^2\rangle \times \langle x_0^2\rangle \\ \langle x'^2\rangle &\overset{\text{def}}{=} \langle x'^2\rangle_{\delta\neq 0} = \langle x'^2\rangle_{\delta=0} + (kl)^2\langle\delta^2\rangle \times \langle x_0^2\rangle \end{aligned} \tag{5}$$

[2]The space charge routine in ASTRA is based on a cylindrical mesh and is not strictly valid for beam spot with large aspect ratio.

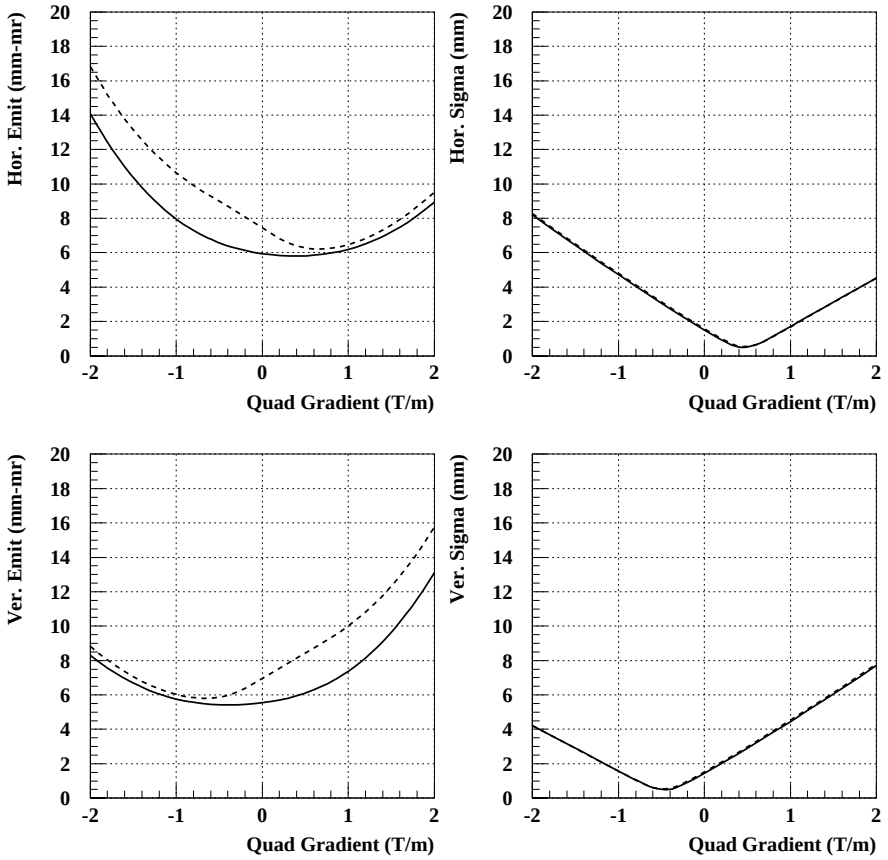

Figure 3: *Simulated variation of transverse emittance and beam spot size at the observation point (INJ.5) versus the quadrupole Q1.INJ1 gradient. The dashed and solid line corresponds to the case of space charge routine activated and not activated, respectively. The beam input distribution used during these simulations is pictured Fig.5.*

$$\langle xx' \rangle \stackrel{\text{def}}{=} \langle xx' \rangle_{\delta \neq 0} = \langle xx' \rangle_{\delta=0} + (k^2 l^2 L) \langle \delta^2 \rangle \times \langle x_0^2 \rangle$$

where $\langle x^2 \rangle_{\delta=0}$, $\langle x'^2 \rangle_{\delta=0}$, and $\langle xx' \rangle_{\delta=0}$ are the usual second order moment transported using the linear transfer matrix (e.g. $\langle x^2 \rangle_{\delta=0} = R_{11}^2 \langle x_0^2 \rangle + R_{12}^2 \langle x'^2_0 \rangle + 2R_{11}R_{12} \langle x_0 x'_0 \rangle$, where the subscript $_0$ denotes the phase space moments at the quadrupole entrance plane). It is worth noting, from Eqn.(5), that chromatic[3] dilution of the beam spot at the observation point is significant provided $k > R_{11}/(\langle \delta^2 \rangle^{1/2} lL)$; this inequality is not fulfilled neither in the simulations nor in the experimental measurements presented in this note. This latter point is of importance: it validates the emittance measurement technique based on the measurement of beam spot sizes at the observation point. However, chromatic emittance growth is not negligible; from Eqn.(5) we get for the squared emittance:

$$\tilde{\varepsilon}_{x,\delta}^2 = \tilde{\varepsilon}_{x,\delta=0}^2 + \langle \delta^2 \rangle (kl)^2 \left[\langle x^2 \rangle + L^2 \langle x'^2 \rangle - 2L \langle xx' \rangle \right] \tag{6}$$

[3]The chromaticity is $\xi = -0.2$ when the quadrupole gradient is set to 2 T/m

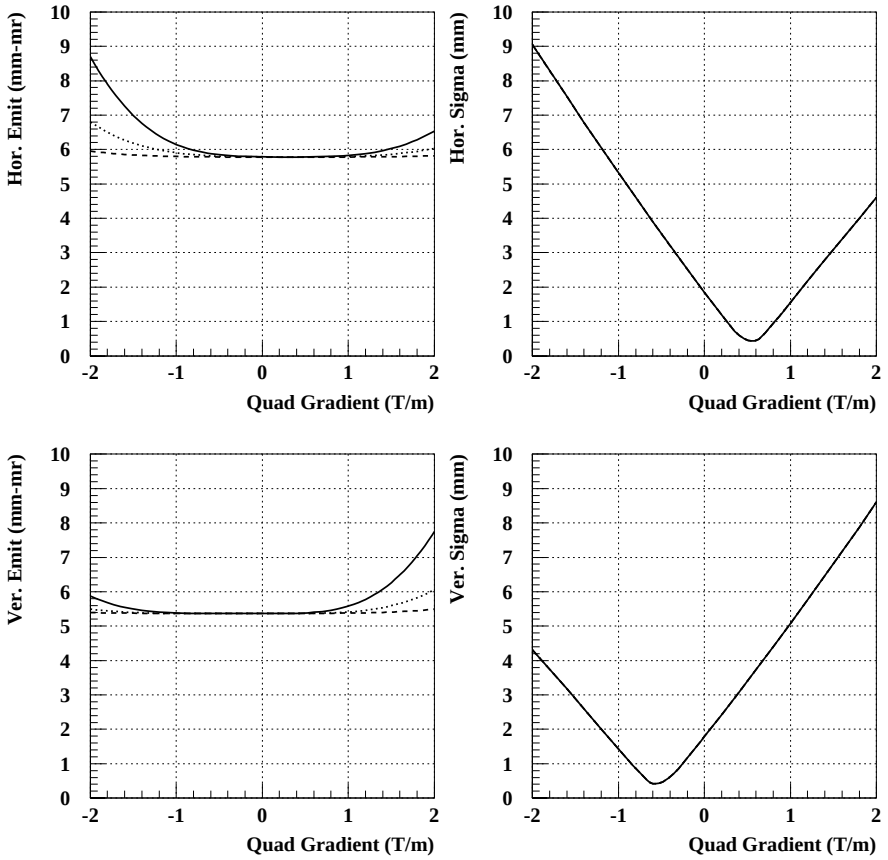

Figure 4: *Simulated variation of transverse emittance and beam spot size at the observation point (INJ.5) versus the quadrupole Q1.INJ1 gradient. The dashed, dotted, and solid line corresponds to the case of different incoming beam rms relative energy spread of 0, 50, and* 150 keV *respectively. The beam input distribution is assumed to be gaussian in the 6D phase space.*

and the second term on the right hand side can be neglected provided:

$$k \ll \frac{\tilde{\varepsilon}_{x,\delta}}{l\langle\delta^2\rangle^{1/2}} \frac{1}{\sqrt{\langle x^2\rangle + L^2\langle x'^2\rangle - 2L\langle x x'\rangle}} \tag{7}$$

This latter inequality is not a fortiori satisfied during our measurements/ simulations so that there is substantial emittance dilution downstream the quadrupole. Nevertheless because of Eqns.(5), the beam spot measurement is still meaningful for an emittance measurement, as already mentioned.

1.2 Experimental Conditions

The "pepperpot"-based transverse phase space measurements occur at z =3.619 m from the photocathode surface, where the multislit mask consisting of horizontal slits allows

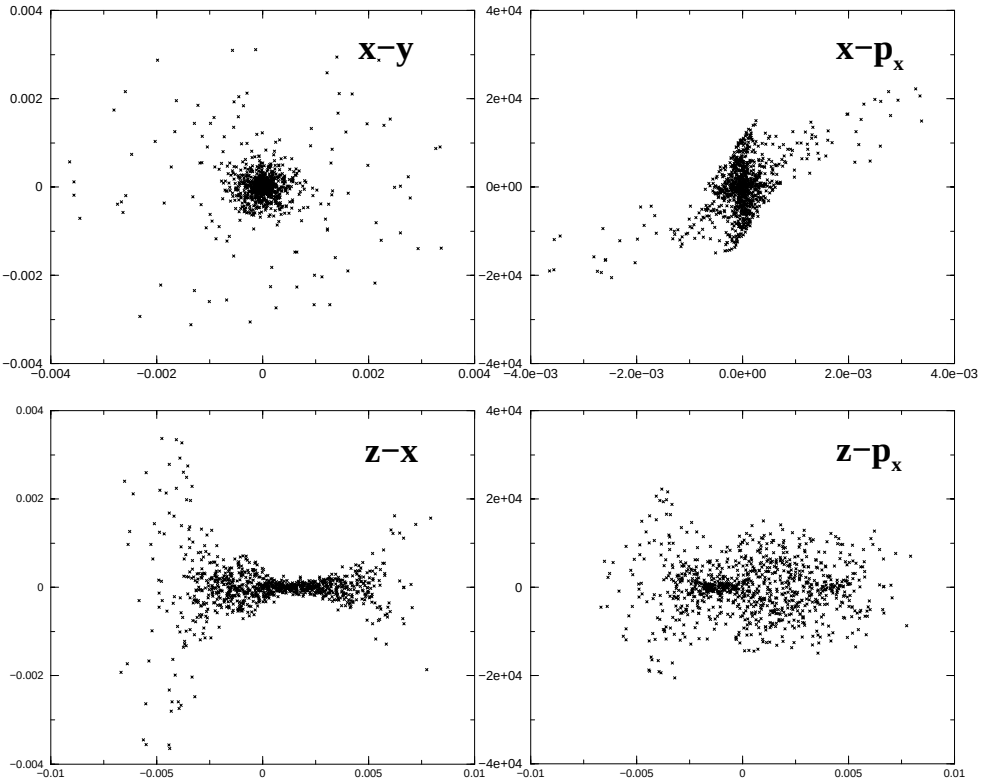

Figure 5: *Initial distribution used at the entrance of the scanned quadrupole in the simulations. The units are meters for x and z, and eV/c for p_x.*

the measurement of the transverse vertical emittance $\tilde{\varepsilon}_y$. Two sets of slits can be inserted into the beam path: one consisting of 0.5 mm slits spacing and the other with 1 mm slits spacing. During the experiment we switched from one set to the other depending on the beam size/divergence at the multislit mask so that we could observed five beamlets at least for all the measurements[4]. The analyzer OTR screen which allows the measurement of the beamlets profiles is located at z =4 m. A gated intensified CCD camera was installed for the measurements.

Concerning the quadrupole scans, the Twiss parameters and emittance values are given at the entrance plane of the quadrupole whose magnetic gradient is being varied, i.e. quadrupole Q1.INJ1 (located at z =2.81 m) in the present experiment (Note that the emittance is implicitly assumed to be a constant quantity along the transport line, because of the single-particle-dynamics assumption on which the quadrupole scan technique relies).

The injector settings used during the December 1999 experiment were as follows:

- the gun phase with respect to the laser was set to −150 deg this corresponds, as shown in Figure 6 (A) to an absolute phase difference between the laser and electric field in the gun of ≃62 deg[5].

[4]for one measurement we were able to resolve a sufficient number of beamlets with both sets we thereby checked the retrieved emittance was independent of the mask used.

[5]The method to compute the absolute operating condition of the gun has recently been improved by one of us (K.F.) to include a Schottky-like dependence of the charge emission on the electric field on the photocathode.

- the gun-solenoids nominal settings were 180 A for the primary solenoid and 93 A for the secondary.
- the photocathode drive-laser was collimated by a circular aperture of 3 mm diameter yielding a uniform beam spot on the photocathode of radius $\simeq$ 1.5 mm. The laser longitudinal profile is assumed gaussian with an rms width of 8 ps.

The injector settings used during the January 2000 experiment were as follows:

- the gun phase with respect to the laser was set to -145 deg this corresponds, as shown in Figure 6 (B) to an absolute phase difference between the laser and electric field in the gun of $\simeq$35 deg.
- the gun-solenoids nominal settings were 210 A for the primary solenoid and 105 A for the secondary.
- the photocathode drive-laser was collimated by a circular aperture of 3 mm diameter yielding a uniform beam spot on the photocathode of radius $\simeq$ 1.5 mm. The laser longitudinal profile is assumed gaussian with an rms width of 8 ps.

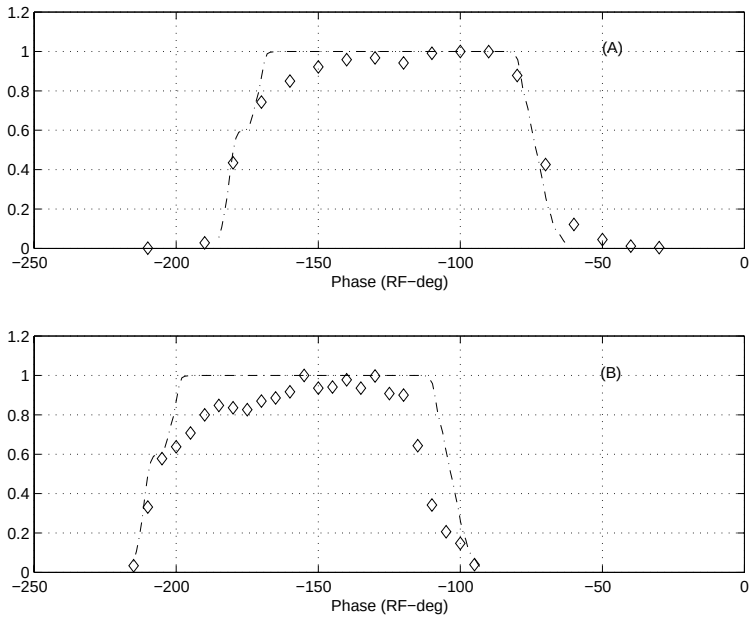

Figure 6: *Bunch charge measured versus phase variation of the photocathode drive laser (diamonds). The dashed lines correspond to simulated data with the proper phase (horizontal axis) offset to match the experimental measurement. From the offset value we can deduce the absolute phase between the gun electric field and the photocathode drive-laser. The data set from Dec,1999* **(A)** *indicates that the absolute phase difference between the laser and the electric field in the gun was approximately* 62 deg, *whereas it was around* 35 deg *during Jan. 2000 measurements* **(B)**

The use of this fitting routine gave similar results (within 5 deg) comparable to the aforementioned results for the gun/laser operating conditions.

2 Transverse Phase Space data taken with the multislit mask

The first measurement occurs on December 15th 1999, where a systematic study of the vertical emittance was performed versus the injection phase between the laser and the gun cavity electric field. The data are compared in Figure 7 with the expected values obtained with ASTRA; though there is substantial disagreement in the low phase-values region, the code reproduces rather well the tendency observed experimentally; it also confirms that the operating point of approximately 60 RF-deg, devised experimentally during operation, does indeed correspond to a minimum (at least for the nominal settings of the gun solenoids). Also for phases smaller than 10 deg, the measured emittance is smaller, a feature that was inferred to scraping [6] and which seems to be confirmed by numerical simulation (only a fraction of the beam is transported to the multislit mask when the phase is lower than approximately 12 deg) [7]. Another series of measurements was performed using the multislit mask on December 17th 1999. At that time the investigation of the effects of the two gun-solenoids settings was conducted. A numerical computation of transverse emittance versus the settings of the two principal gun-solenoids is shown in figures 8 and 9; it especially enlight an "emittance valley", which in turn indicates there is a family of settings which allow the transverse emittance to be (locally) minimized. For clarity we compared the measured vertical emittance, rms beam divergence and rms beam size in Figures 10, 11 and 12. The same remarks as previous still yield: the code has again captured the tendency of the transverse parameters evolution versus the primary and secondary gun solenoid settings we have experimentally observed. At this point, it is worth mentioning that the simulation were executed posteriorly to the experiment and thus we were not aware, during the experiment, of the large increase in emittance for large secondary solenoid peak field, that is the reason we did not explore the corresponding region.

3 Emittance Measurements with the Quadrupole Scan Method

The measurements were performed on 6 and 7 January with experimental condition close to the one used December 17th and 19th, 1999 apart from the gun phase. During the measurements, the gun voltage was varied by approximately 7%. The emittance, rms beam size and divergence are plotted in Figure 7 for comparison with the data taken with the multislit mask; the agreement between the two method is quite good, and the data are even closer to the values predicted by ASTRA.

Another study that was conducted consisted in varying the gun "trim solenoid" to vary the magnetic field at the photocathode surface, the expected variation over the full range of trim solenoid is approximately 0.1 T; we compare in Figure 13 the data measured for two different gun primary and secondary solenoids settings, with ASTRA simulations where we assumed the magnetic field is zero on the photocathode. It seems

[6] Although the beam current was not constantly monitored during the measurement so no clear evidence of beam scraping was experimentally established

[7] Taking into account the dependence of charge emission w.r.t to gun electric field on the photocathode, similar results (within few percents) have been obtained for phase above 20 deg. However below this value, the charge emitted is lower; this yields (1) a lower emittance, and (2) the absence of scraping.

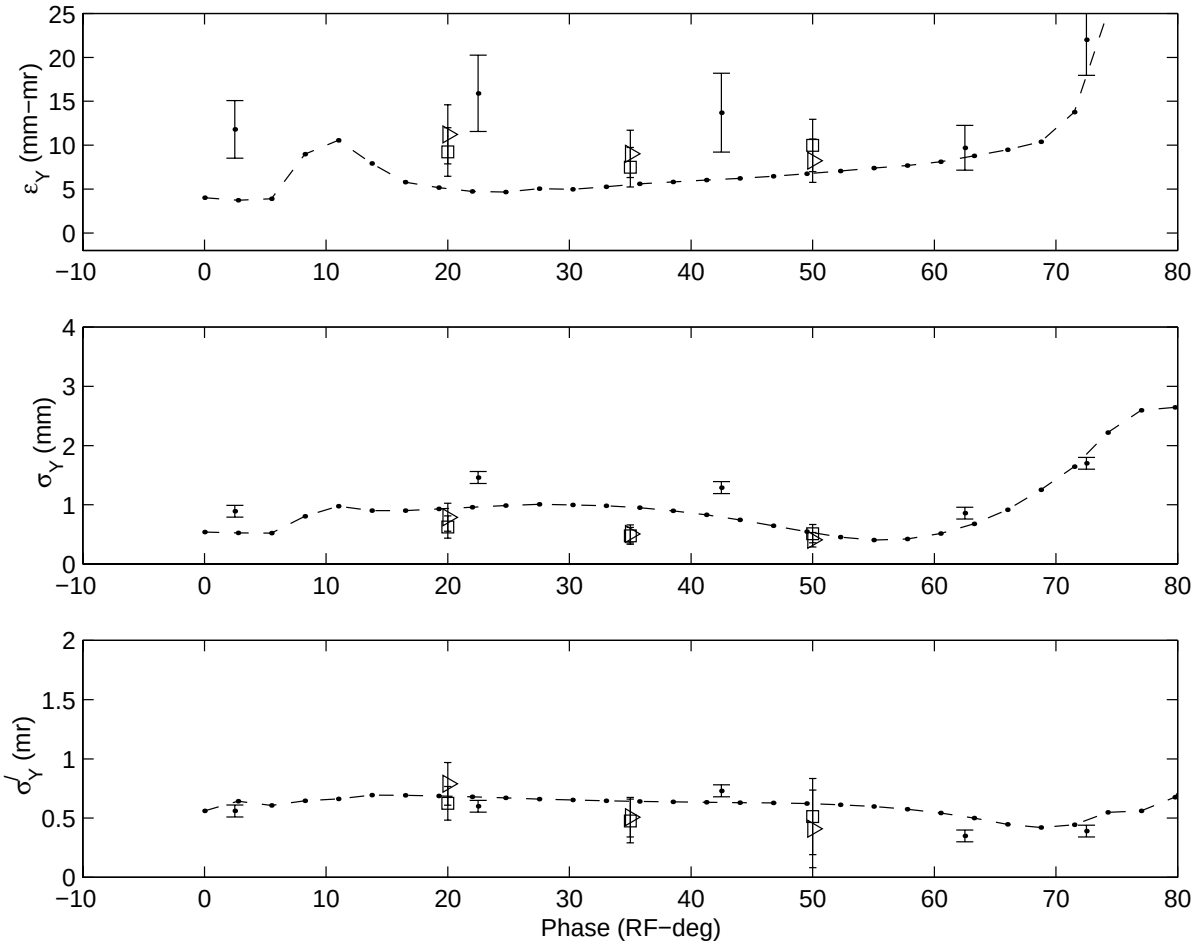

Figure 7: *Comparison of experimentally measured and numerically computed values of the vertical rms emittance* $\tilde{\varepsilon}_y$ **(top)**, *beam size* σ_y **(middle)**, *and beam divergence* σ'_y **(bottom)** *versus the absolute injection phase of the photocathode drive-laser. The dot-dashed lines are results of simulations performed with* ASTRA, *the dots data-points are taken with the "pepperpot" method, and the Square and Triangle data represent respectively the vertical and horizontal emittance measured with the quadrupole scan technique respectively. Note that the spot size is not measured directly in the case of the pepperpot measurement.*

the trim solenoid does not have any significant contribution to emittance, at least for the presently (relatively large, $\simeq$5 mm-mr), measured emittance, and within the accuracy of the emittance measurement. The magnetic contribution to emittance, $\tilde{\varepsilon}_{MAG}$, induced by the presence of a non-zero magnetic field, B_z, on the photocathode is expected to scale linearly with the magnetic field as:

$$\tilde{\varepsilon}_{MAG} = \frac{e}{8 m_e c^2} B_z r^2 \tag{8}$$

where the transverse beam distribution on the photocathode is assumed to be a uniform distribution with radius r. For r =1.5 mm this results in a magnetic contribution to transverse emittance (in mm-mr units) of approximately $\tilde{\varepsilon}_{MAG} = 165 \times B_z$ (with B_z expressed in Tesla units). Typical values of B_z on the photocathode are of the order of mT so that

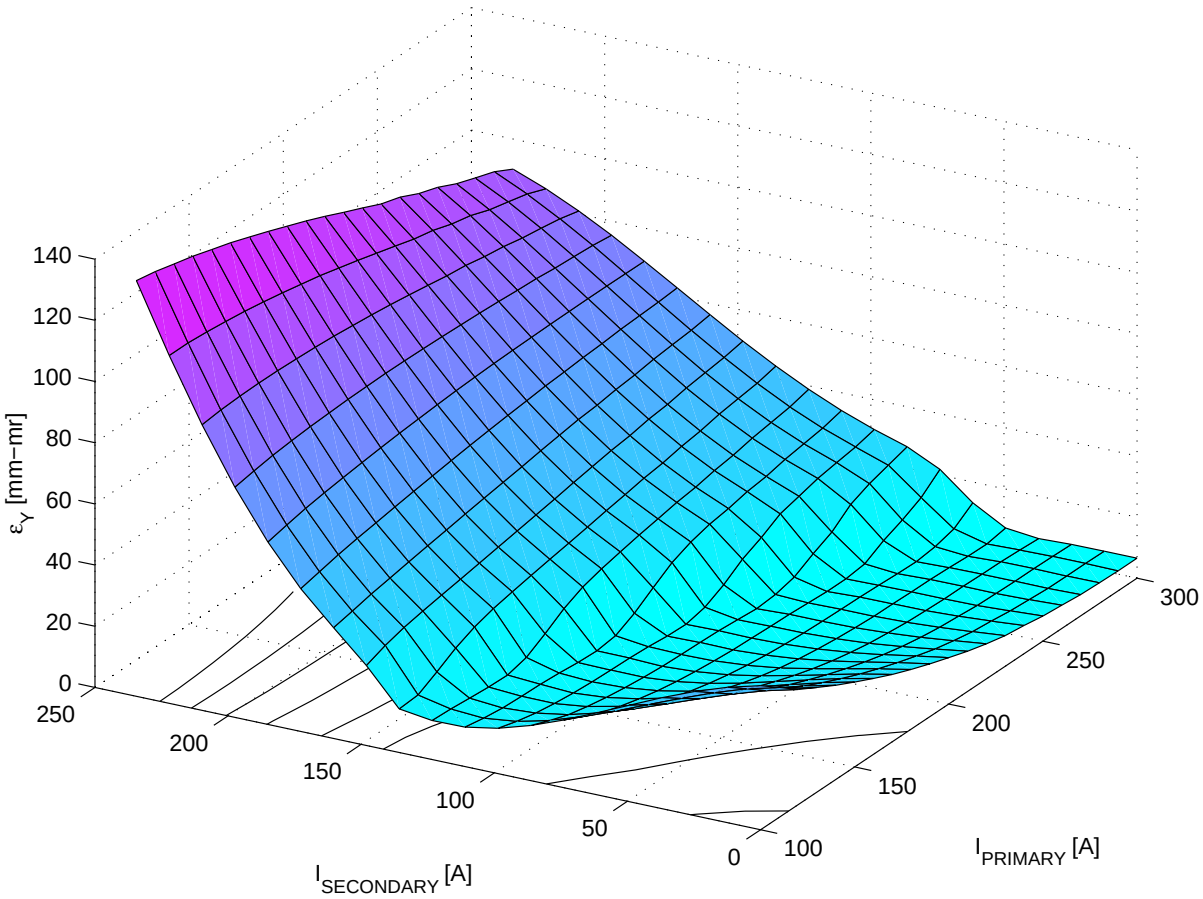

Figure 8: *transverse emittance at the pepperpot measurement location versus excitation of primary and secondary gun-solenoids.*

the contribution to the total emittance is negligible since it must be added quadratically.

A final measurement consisted in varying the primary and secondary gun solenoid in the ratio 1:1/2 and measuring emittance; this later measurement is compared with ASTRA simulations in Figure 14, here we observe a good agreement between measurement and simulation.

4 Transverse x-y beam density Measurement

4.1 Beam density versus gun solenoids settings

Using a 12-bit CCD camera we have measured, on December 15th 1999, the x-y beam density using optical transition radiation. The beam spots measurements are gathered along with the beam profiles in Figure 16, the expected beam spots and profiles are presented in Figure 15. The main disagreement resides in the beam aspect ratio: at the time of this measurement the measured beam spot is not axi-symmetric as it should be since all the external forces are axi-symmetric.
There are many effects that could yield such observations, for instance: (1) the mirrors guiding the laser beam on the photocathode were found to get charged ,as dark current

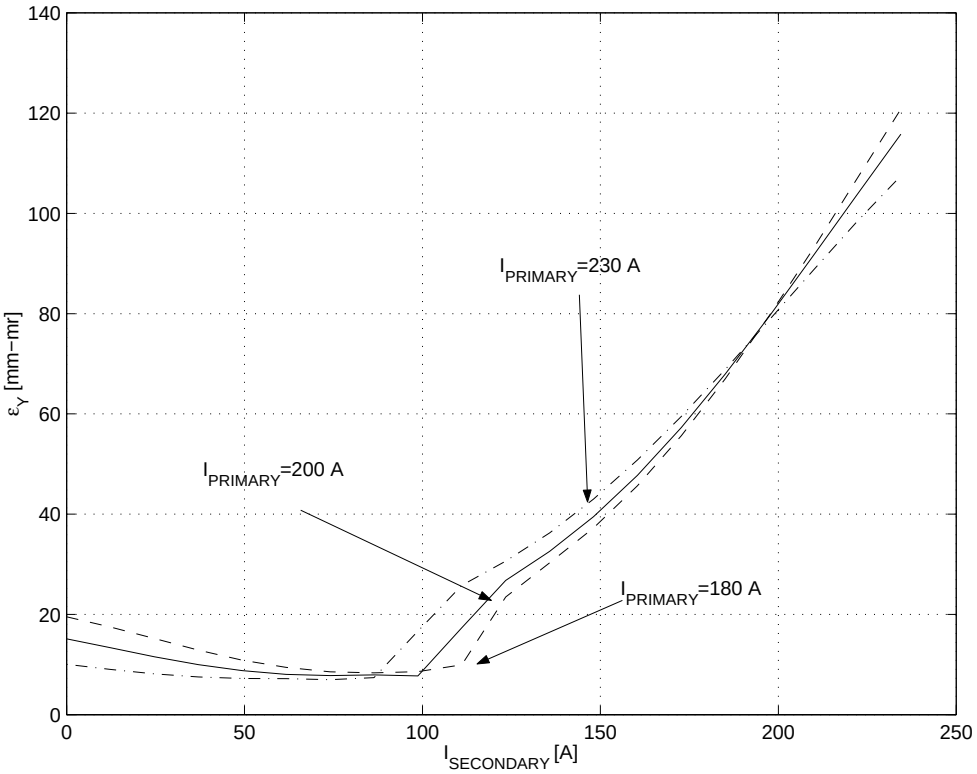

Figure 9: *Cut of the surface plotted in Fig. 5 for solenoids settings close to the nominal operating point.*

was scraped on them, thereby steering the beam (but this effect might as well have other consequences, e.g., on the beam envelope [8]), (2) the beam might be misaligned in the solenoid so that varying the solenoid strength also induces some steering effects which in turn might results in misalignment in the booster cavity and leads to aberrations in the transverse plane; (3) the beam might be subject to transverse RF-kick in the booster cavity due to the RF-fields asymmetry in the vicinity of the input and high order modes (HOMs) couplers; such transverse field will break the beam symmetry but also induce some transverse aberration via head-tail type effects.

4.2 Beam density versus quadrupole settings

We have not yet performed a full parametric study of the beam spot changes versus quadrupole settings in the injector area. However we were able to perform preliminary measurement for two different injector settings of the beam density in the x-y plane on the screen 1INJ6. The results are compared in figure 17. Qualitatively, the measured and simulated beam spots exhibit the same type of pattern (simulation were performed by tracking 5000 macroparticles with ASTRA).

[8] This point seems to be supported by recent measurements with a new set of mirror (which are supposed not to be strongly subject to the "charging-up" problem): the beam spot size are in better agreement with our simulations.

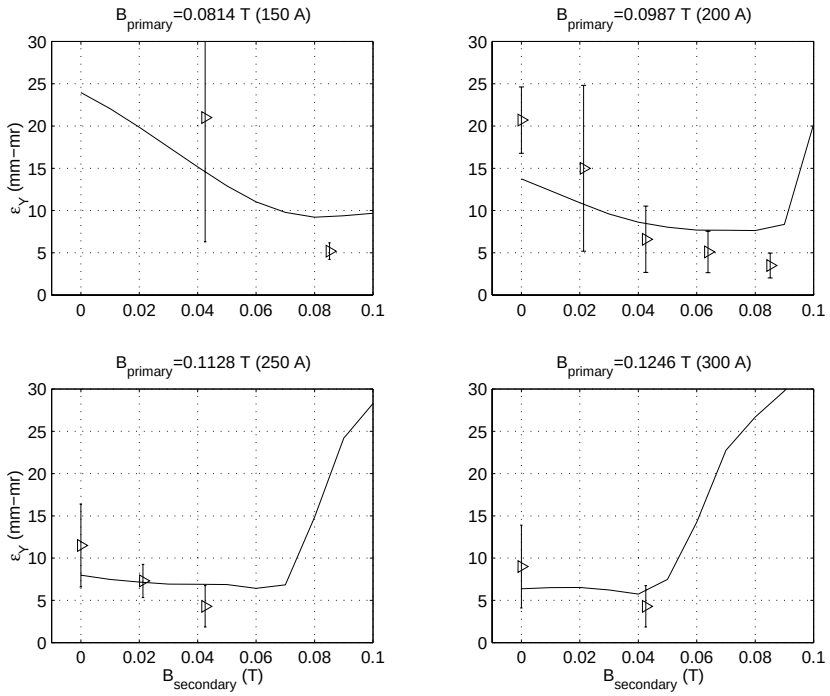

Figure 10: *Comparison of experimentally measured and numerically computed values of the vertical rms emittance $\tilde{\varepsilon}_y$ for different settings of the primary and secondary gun solenoids.*

5 Conclusion

We believe we have presently a rather good understanding of the transverse Beam Dynamics in the injector from the photocathode up to the booster cavity exit: emittance evolutions versus several beam parameters is reproduced rather well by the simulation code ASTRA; discrepancies are still observed for certain cases, and we believe some of them might be attributed to the unknown consequences of the "charging effect" of the mirrors used to guide the photocathode laser up to the photocathode during run#00-01. There is also still points that needs to be improved in both experiment and the simulation tool.

On the experimental point of view, it is important to measure the beam laser spot density on the photocathode, and to do autocorrelation of the laser pulse. The experimental station to measure transverse emittance using the pepperpot has recently been improved by replacing the OTR foil with a YaG screen; this should provide much more light so that we could avoid using an intensified camera that cannot be permanently installed in the accelerator enclosure (because of radiation-induced damages).

On the other hand, the tracking code ASTRA is currently being refined to incorporate more detailed modeling: space charge routines for asymmetric beam, tracking in full 3D-electromagnetic map provided by the MAFIA-E3 module, and implementation of wakefield are under consideration.

Finally, it is worth mentioning that a complete picture of the Beam Dynamics requires

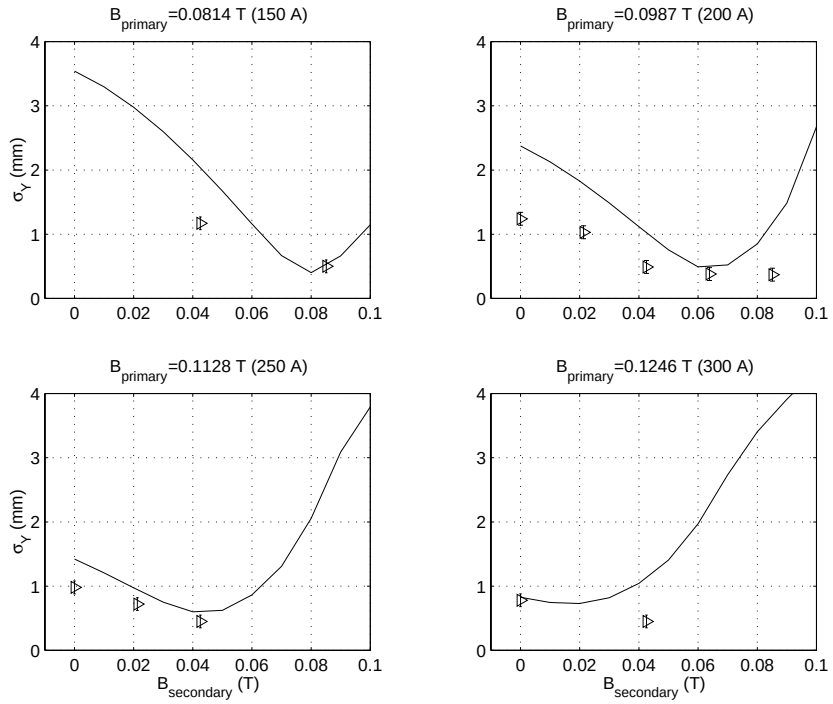

Figure 11: *Comparison of experimentally measured and numerically computed values of the vertical rms beam size σ_y for different settings of the primary and secondary gun solenoids. Note that the spot size is not measured directly in the case of the pepperpot measurement*

both transverse and longitudinal beam parameters to be measured at the same time. The series of measurement presented in this note are planned to be repeated with the new photocathode laser guiding mirrors that have been installed in April 2000.

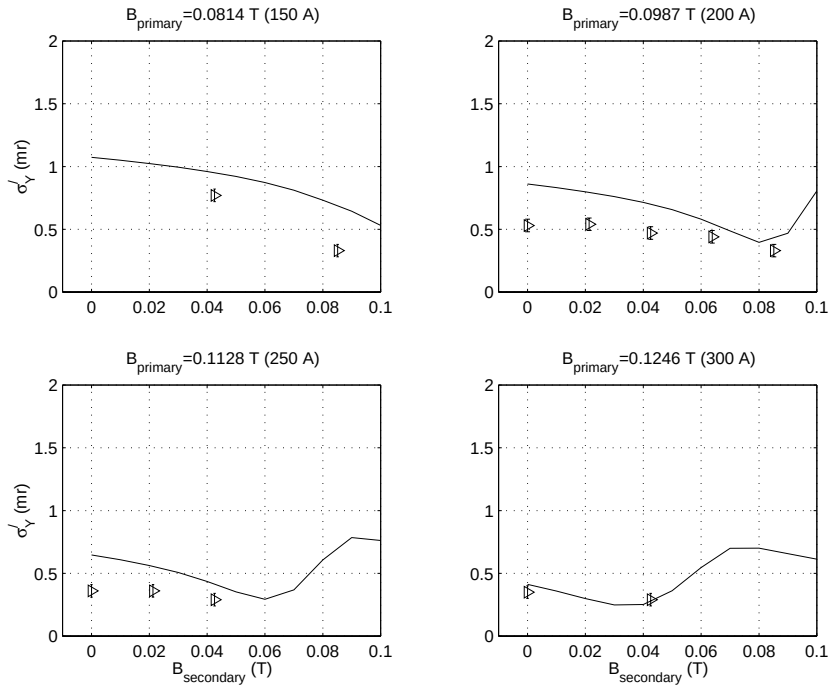

Figure 12: *Comparison of experimentally measured and numerically computed values of the vertical rms beam divergence σ'_y for different settings of the primary and secondary gun solenoids.*

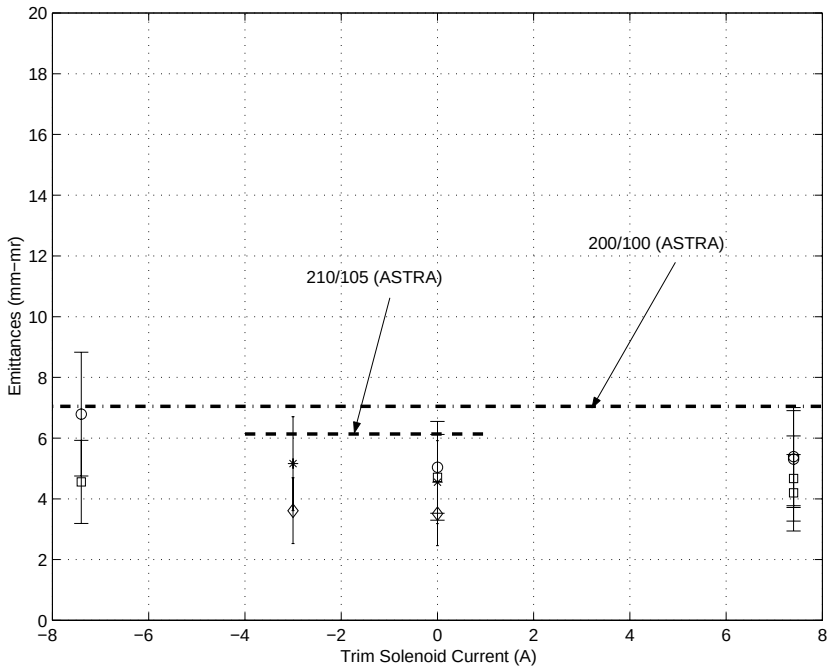

Figure 13: *Transverse emittances versus gun "Trim solenoid" settings for two different gun solenoids settings. Dashed lines are simulation results obtained with* ASTRA *(the number indicates the settings of primary/secondary solenoids). Circles and Squares are measured horizontal and vertical transverse emittances respectively for the gun solenoid settings 200/100. Triangles and Stars are measured horizontal and vertical transverse emittances for the gun solenoid settings 210/105 respectively.*

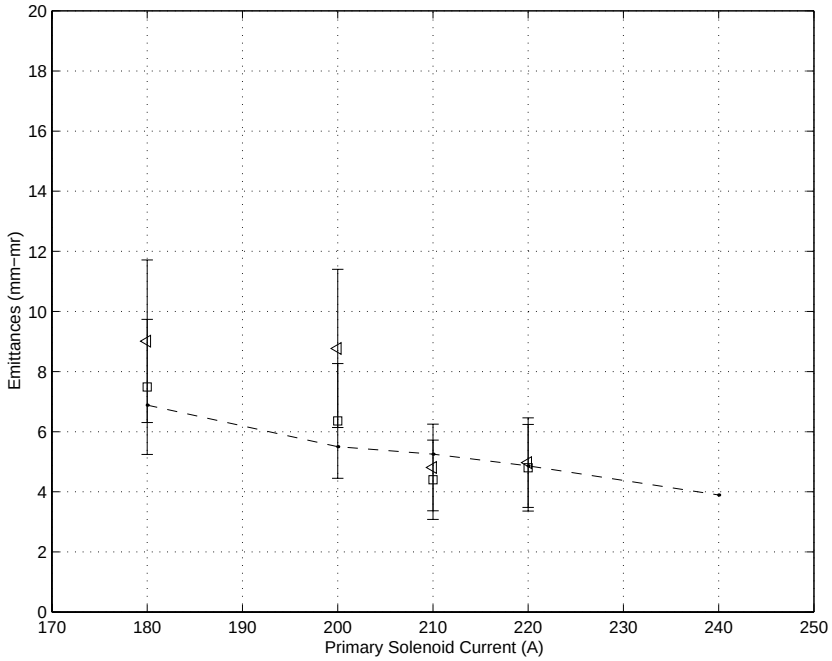

Figure 14: *Transverse emittance versus primary gun-solenoid current excitation, during the measurement the secondary solenoid current is set to half of the primary solenoid current. Squares and Triangles represent measured points (horizontal and vertical emittance respectively). Dashed line is result from* ASTRA *simulation.*

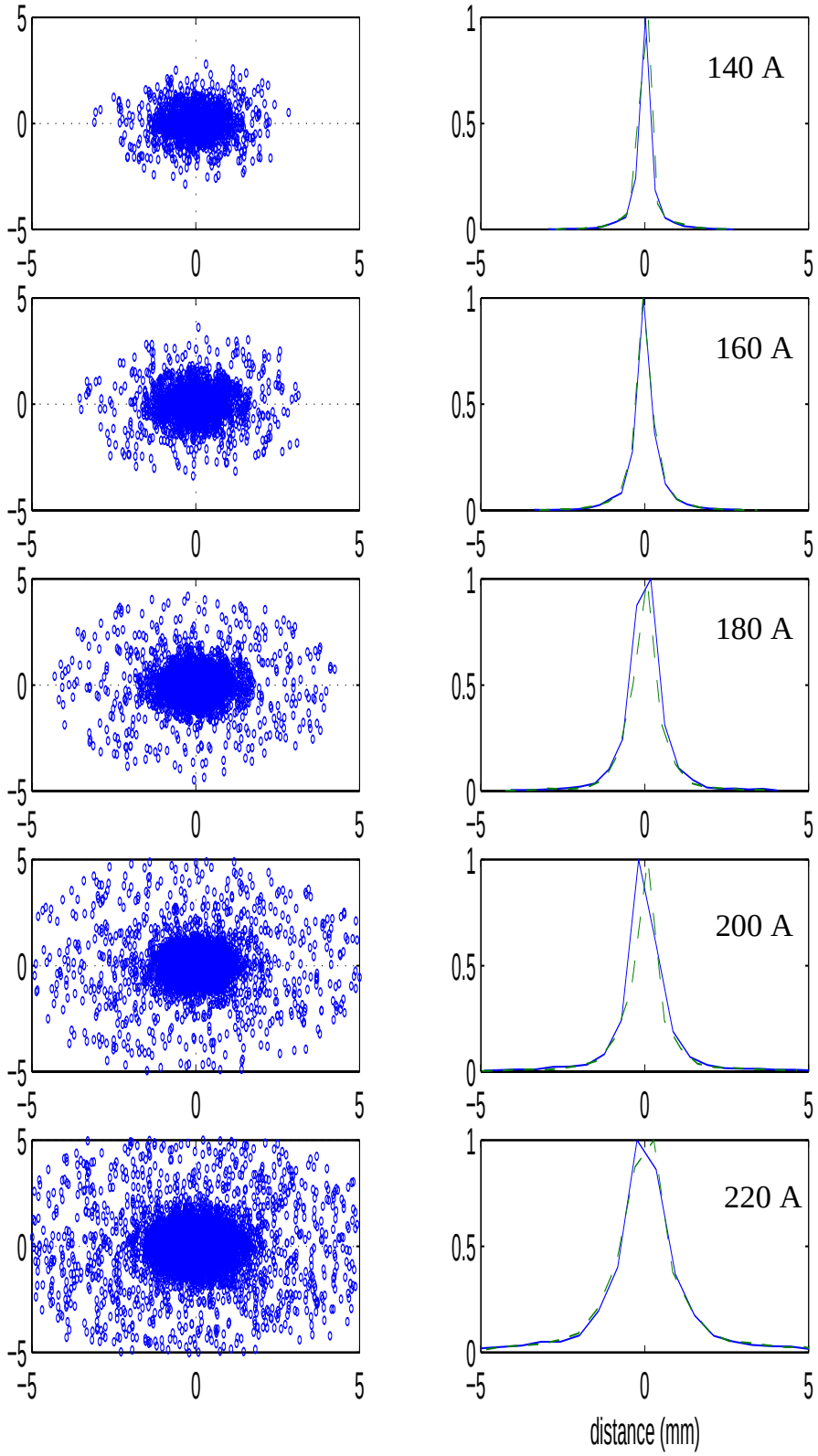

Figure 15: *Simulated beam density* **(left plots)** *and deduced transverse profiles* **(right plots)** *for different solenoid settings. The primary/secondary current values (from top to bottom) are: 140/93, 160/93, 180/93, 200/93 and 220/93 Ampères. The solid and dashed lines correspond to the horizontal and vertical beam profile respectively.*

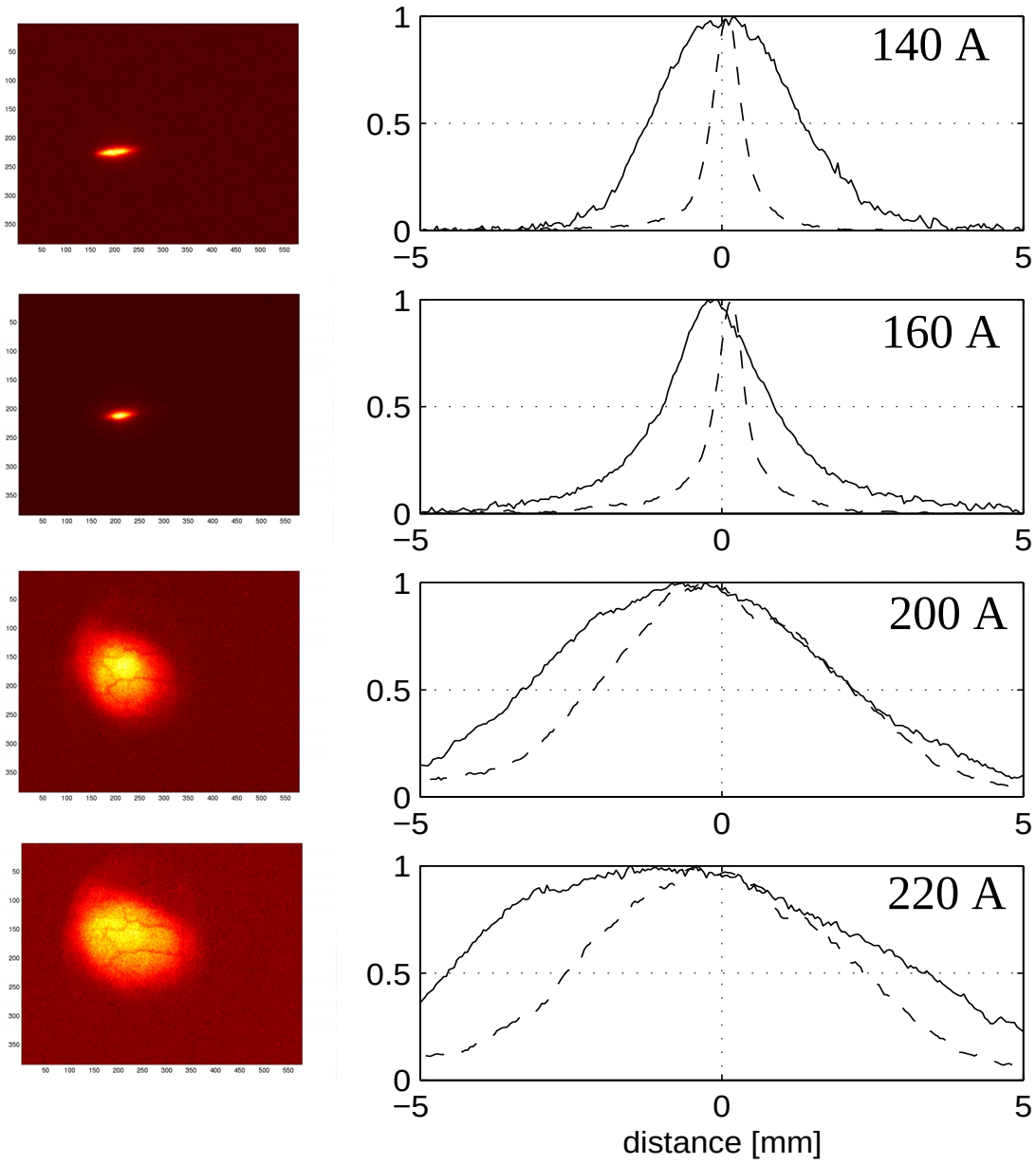

Figure 16: *Measured beam density* **(left plots)** *and deduced transverse profiles* **(right plots)** *for different solenoid settings. The primary/secondary current values (from top to bottom) are: 140/93, 160/93, 200/93, and 220/93 Ampères. The solid and dashed lines correspond to the horizontal and vertical beam profile respectively.*

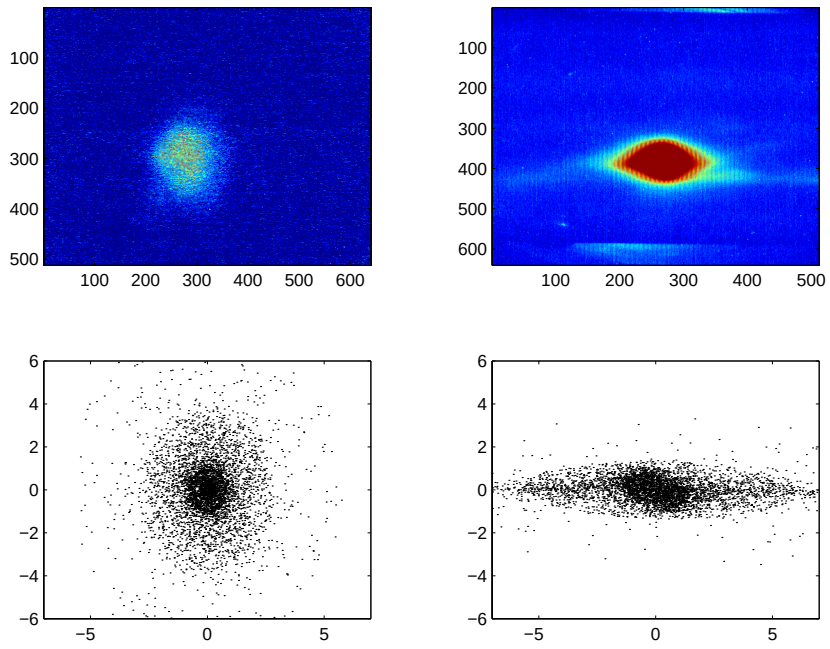

Figure 17: *Comparison of experimentally measured (***top***) and numerically computed (***bottom***) beam spots on the OTR density monitor 1INJ6 with the injector quadrupoles turned off (***left***) and excited to their nominal settings (***right***). Both the experimental and simulated pictures have the same sizes. The distance mentioned on the bottom picture are mm.*

References

[1] K. Floettmann, *Astra User Manual*

[2] E. Colby, in proceeding of LINAC'98 report **ANL-98-28** vol. 2, pp. 758-762 (1998)

[3] See for instance M. Reiser, *Theory and Design of Charged Particle Beam*, John Wiley & Sons Edt., p. 363 (1994). For the orginal derivation see F. Sacherer, CERN report CERN internal report, **SI/DL/70-12** (1970)